AGU PUBLICATIONS

Global Biogeochemical Cycles

RESEARCH ARTICLE
10.1002/2016GB005554

Key Points:
- The 2013 U.S. GEOTRACES Eastern Pacific Zonal Transect (EPZT) traversed the highly productive Peruvian coastal upwelling region (PCU)
- The cosmogenic isotope ^{7}Be was used to estimate upwelling rates and vertical diffusivity in the upper thermocline of the PCU
- The ^{7}Be-derived vertical transport terms were applied to nitrate profiles to derive net community production

Correspondence to:
D. Kadko,
dkadko@fiu.edu

Citation:
Kadko, D. (2017), Upwelling and primary production during the U.S. GEOTRACES East Pacific Zonal Transect, *Global Biogeochem. Cycles*, *31*, doi:10.1002/2016GB005554.

Received 17 OCT 2016
Accepted 9 JAN 2017
Accepted article online 11 JAN 2017

©2017. American Geophysical Union. All Rights Reserved.

Upwelling and primary production during the U.S. GEOTRACES East Pacific Zonal Transect

David Kadko[1]

[1]Applied Research Center, Florida International University, Miami, Florida

Abstract The 2013 U.S. GEOTRACES Eastern Pacific Zonal Transect (EPZT) traversed the highly productive Peruvian coastal upwelling (PCU) region. In this work, the flux of nitrate into the euphotic zone is derived for stations within the PCU using a previously developed method whereby dilution of the water column ^{7}Be inventory by upwelled ^{7}Be-free water provides a means to infer upwelling rates. Furthermore, with knowledge of upwelling rates, ^{7}Be profiles are used to constrain vertical diffusivity within the upper thermocline. These transport terms are applied to nitrate profiles to estimate net community production between 79°W and 104°W along the EPZT, which includes the zone of active upwelling to the edge of the oligotrophic gyre. With a simple, one-dimensional model, the calculated upwelling rates were inversely related to mixed layer temperature and ranged from 0 to 3.0 m/d. Results using a depth-dependent upwelling rate with a component of horizontal advection are also described. Vertical diffusivities near the base of the euphotic zone were in the range $1.7–4.5 \times 10^{-4}$ m^2/s. These values are compared to those generated by analysis of temperature profiles. Net community production averaged 15 mmol C/m^2/d for stations between 84°W and 104°W and was 134 mmol C/m^2/d for the furthest inshore station at 79°W which displayed the lowest SST and greatest rate of upwelling.

1. Introduction

The southeastern tropical Pacific along the west coast of South America is one of the most biologically productive regions in the world, supporting an important fishery and large seabird population [e.g., *Chavez and Barber*, 1987; *Fiedler et al*., 1991; *Pennington et al*., 2006; *Montecino and Lange*, 2009]. The biological richness here contrasts that within the low-productivity oligotrophic waters of the adjacent mid-ocean gyre. High primary production is driven by upwelling that provides the euphotic zone with an abundant supply of inorganic plant nutrients and drives significant carbon export. An oxygen-deficient zone (ODZ) beneath these productive waters is fueled by the respiration of the sinking particles supplied from above [e.g., *Karstensen et al*., 2008; *Fuenzalida et al*., 2009]. In 2013, the U.S. GEOTRACES Eastern Pacific Zonal Transect (EPZT) traversed the highly productive Peruvian coastal upwelling region (PCU) which is characterized by the lowest sea surface temperature (SST), highest mean surface nitrate and phosphate, highest average surface chlorophyll concentration, and greatest rate of primary productivity of the eastern tropical Pacific [*Pennington et al*., 2006]. Estimating new production here, and in similar regions, is important to understanding the ecosystem function of fisheries, the nature of ODZs, and the role of upwelling regions in the planetary carbon cycle.

Here rates of upwelling and vertical diffusion are estimated within the PCU using a previously developed method based on water column measurements of ^{7}Be. These transport terms are applied to nitrate profiles to estimate net community production between 79°W and 104°W along the EPZT, which includes the zone of active upwelling to the edge of the oligotrophic gyre.

Beryllium-7 is a cosmic ray-produced isotope (half-life = 53.3 days) that is deposited upon the ocean surface primarily by rainfall and subsequently homogenized within the surface mixed layer [e.g., *Silker*, 1972; *Aaboe et al*., 1981; *Young and Silker*, 1980; *Kadko and Olson*, 1996; *Kadko*, 2000, 2009]. In the absence of physical removal processes other than radioactive decay, the water column inventory of the isotope represents an integration of the atmospheric input flux over approximately the previous mean life (77 days) of the isotope [e.g., *Aaboe et al*., 1981; *Kadko and Prospero*, 2011; *Kadko et al*., 2015]. The ^{7}Be flux and water column inventory vary as a function of rainfall and over broad oceanic regions are relatively constant. This is manifested by the observation that water column inventories are inversely related to surface salinity [*Young and Silker*, 1980; *Kadko and Olson*, 1996; *Kadko and Johns*, 2011]. In regions of upwelling, the ^{7}Be inventory will be diluted by the penetration of ^{7}Be-free water brought up from below. The dilution of the ^{7}Be inventory provides a

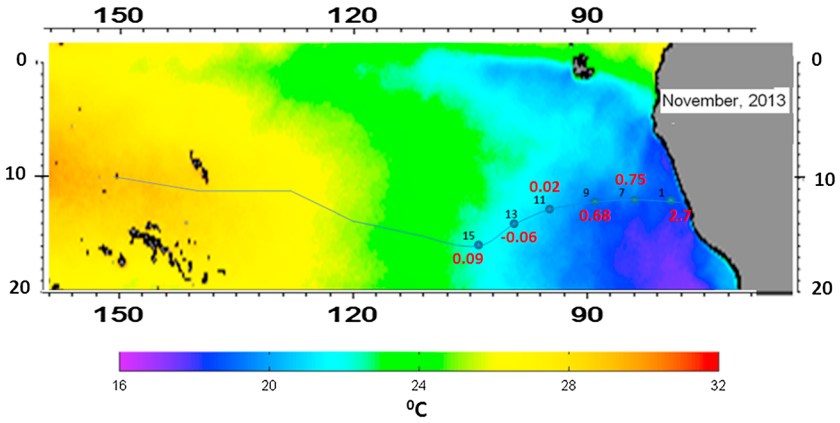

Figure 1. Cruise track of the U.S. GEOTRACES East Pacific Zonal Transect (EPZT) expedition from the R/V *Thomas G. Thompson* (TGT303, 25 October 2013 to 20 December 2013, Manta, Ecuador, to Papeete, Tahiti) superimposed over a thermal infrared multispectral scanner (TIMS) map of SST. Stations sampled for ^{7}Be discussed in this work are indicated. Red numbers are upwelling rates (m/d) determined from equation (2), for $u = 0.1$ m/s (see text).

means to infer upwelling rates, and with knowledge of upwelling rates, the shape of the ^{7}Be profiles can be used to constrain vertical diffusivity within the upper thermocline [*Kadko and Johns*, 2011; *Haskell et al*., 2015].

2. Methods

Samples were collected during the U.S. GEOTRACES EPZT expedition from the R/V *Thomas G. Thompson* (TGT303, 25 October 2013 to 20 December 2013, Manta, Ecuador, to Papeete, Tahiti) along the cruise track shown in Figure 1. Beryllium-7 was analyzed by procedures described in detail elsewhere [*Kadko and Johns*, 2011]. Briefly, samples were collected at selected depths by pumping 400–700 L of seawater via a 1.5 inch hose into large plastic barrels on deck. From these barrels, the seawater was then pumped through iron-impregnated acrylic fibers at ~10 L/min [*Lal et al*., 1988; *Krishnaswami et al*., 1972; *Lee et al*., 1991]. The efficiency of the fiber for extraction of Be from seawater was determined by adding 500 mL of a 1000 ppm Be atomic absorption standard to a drum containing seawater. The seawater was pumped through an iron fiber cartridge, and at every 100 L, the Be content of the cartridge effluent was measured by atomic absorption. From these data, the integrated Be extraction efficiencies were calculated. For sample volumes in the range 400–700 L, the extraction efficiencies were respectively 82–76%. On land, the fibers were dried and then ashed. The ash was subsequently pressed into a pellet (5.8 cm diameter) and placed on a low-background germanium gamma detector. The ^{7}Be has a readily identifiable gamma peak at 478 keV. The detector was calibrated for the pellet geometry by adding a commercially prepared mixed solution of known gamma activities to an ashed fiber, pressing the ash into a pellet, and counting the activities to derive a calibration curve. The uncertainty of the extraction efficiency (4%) and the detector efficiency (2%) was in all cases smaller than the statistical counting error and the uncertainty in the blank.

3. Results and Discussion

The ^{7}Be data are presented in Table 1. Samples were collected from the surface mixed layer and from depths within the upper thermocline based on temperature profiles from conductivity-temperature-depth casts made immediately prior to sample collection. These data were used to estimate the total water column inventory of ^{7}Be at sites where, based on temperature, strong upwelling was anticipated, as well as where upwelling was expected to be weak or zero.

Across the study section, ^{7}Be activity in the mixed layer exhibited a total variation of about a factor of 3, between low values of 63.1 dpm/m^{3} found within the Peruvian coastal upwelling zone associated with cooler SST and high values of ~190 dpm/m^{3} associated with warmer SST offshore of the coastal zone. The cooler temperatures along the Peruvian margin are associated with coastal upwelling where alongshore winds produce offshore Ekman transport of surface water which must be replaced by subsurface water to maintain mass balance. The thermocline shoals onshore to $<$40 m and very often breaks the surface, resulting in very

Table 1. ^{7}Be Water Column Data

Station	Lat-Long	Depth (m)	^{7}Be (dpm/1000 L)	ML Temp. (°C)	Station Inventory (dpm/m^{2})
1	12°S-79.195°W	22.5	63.1 ± 12.0	17.62	5060 ± 440
		53	57.5 ± 10.0		
		77	38.6 ± 10.6		
		92.5	15.7 ± 10.7		
		107.5	3.12 ± 6.78		
		122	16.1 ± 10.1		
7	12°S-84°W	23.5	112 ± 18.2	18.92	10,100 ± 630
		45.5	83.1 ± 10.1		
		58.5	95.4 ± 12.1		
		73	88.7 ± 11.0		
		93.5	49.3 ± 8.96		
		113.5	27.2 ± 7.25		
9	12°S-89°W	22.5	118.6 ± 14.0	19.1	13,070 ± 620
		54	140.5 ± 11.5		
		73	103.6 ± 14.2		
		92	101.0 ± 12.5		
		109	51.7 ± 15.1		
		124.5	33.6 ± 10.8		
11	12°S-94°W	13	157.0 ± 18.5	20.92	17,020 ± 670
		51.5	147.7 ± 16.1		
		73.5	130.9 ± 16.0		
		89.5	141.3 ± 17.2		
		105.5	94.0 ± 15.2		
		124.5	48.8 ± 11.6		
13	14°S-99°W	22.5	190.1 ± 17.8	21.26	18,600 ± 770
		52.5	170.6 ± 18.4		
		72.5	152.7 ± 22.8		
		87	110.3 ± 17.4		
		105	80.9 ± 19.8		
		123	41.2 ± 13.7		
15	16°S-104°W	23	166.3 ± 20.2	22.4	19,670 ± 1050
		58.5	184.2 ± 16.3		
		83.5	136.7 ± 22.6		
		103.5	109.5 ± 16.7		
		119.5	54.0 ± 13.8		
		149	32.6 ± 12.6		

low sea surface temperatures for these latitudes [e.g., *Brink et al*., 1983; *Huyer et al*., 1987; *Fiedler and Talley*, 2006; *Pennington et al*., 2006].

The decrease in mixed layer ^{7}Be activity with decrease in temperature occurs as ^{7}Be-"dead", cold, nutrient-rich water is upwelled from below. Profiles comparing temperature and ^{7}Be from upwelling and adjacent nonupwelling stations clearly show the deficit of ^{7}Be in the upwelling water column where deep colder water reaches the surface (Figure 2). This is reflected in the enrichment of nutrients as well. Figure 3 shows ^{7}Be water column activities and depth-integrated inventories plotted against temperature. The linear relationship of these quantities within the upwelling zone attests to the conservative nature of ^{7}Be over the timescale of upwelling in which particulate loss of ^{7}Be can be ignored. This is consistent with earlier findings in the upwelling environment of the equatorial Atlantic [*Kadko and Johns*, 2011], as well in the region of this study [*Haskell et al*., 2015]. With an increase in temperature, the ^{7}Be inventory increases, as the offshore nonupwelling stations are approached. As shown by *Kadko and Johns* [2011], the dilution of the ^{7}Be inventory in upwelling stations relative to the nonupwelling stations provides a measure of the upwelling rate.

3.1. Estimating Upwelling Rates

Upwelling rates are difficult to determine by direct measurement because of the relatively small velocities involved but can be inferred by indirect methods such as those provided by tracer observations. Such tracers derive from the presence, in surface water, of properties characteristic of thermocline water which have been emplaced by the upwelling process. Examples include surface anomalies in ^{14}C, δ^{13}C, apparent oxygen

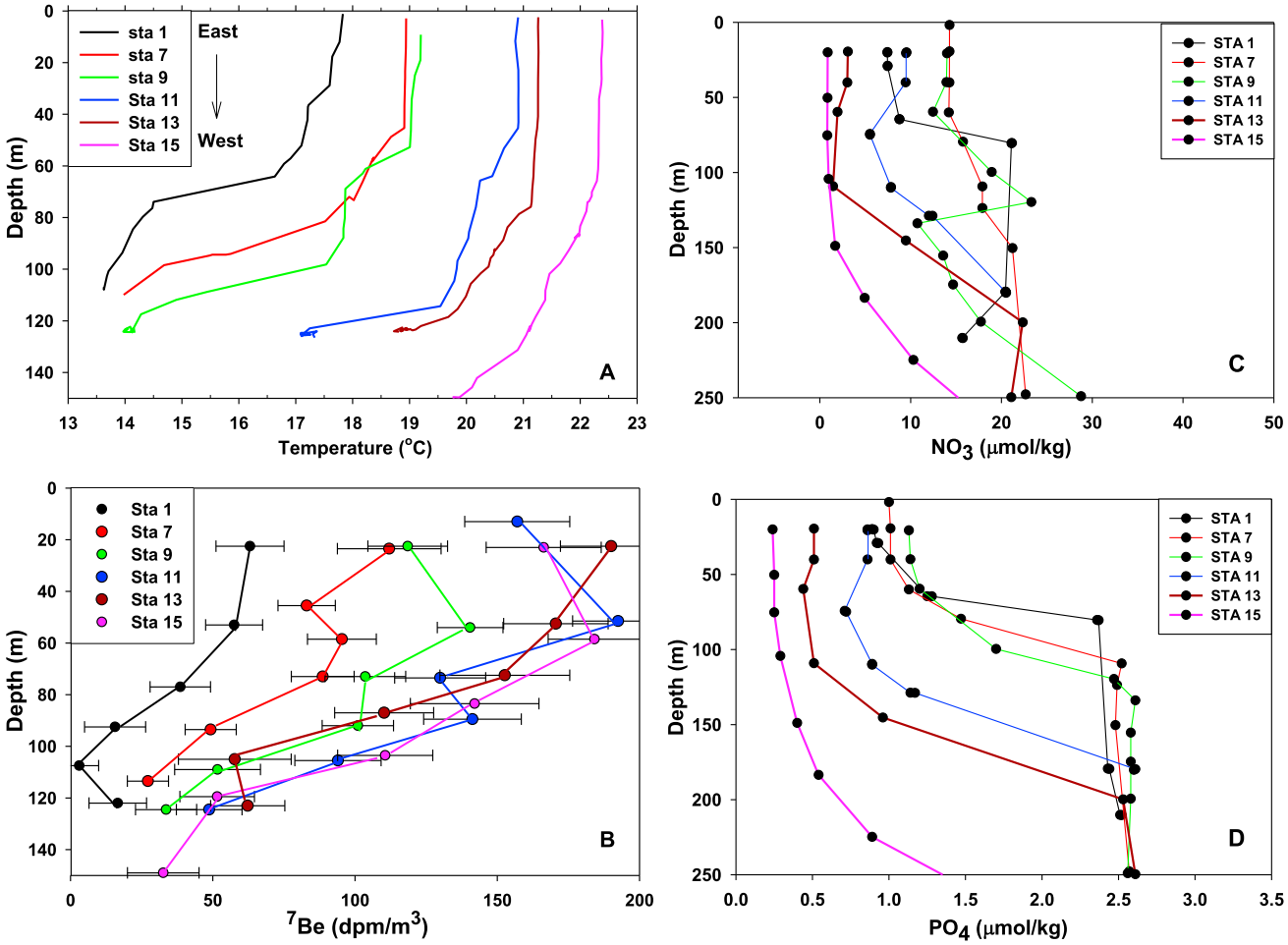

Figure 2. (a) Temperature, (b) ^{7}Be, (c) nitrate, and (d) phosphate plotted versus depth for the stations indicated in Figure 1. Note the gradient in properties moving west from the Peruvian upwelling zone.

utilization, δ^{3}He, ^{7}Be, pCO_2, ΣCO_2, and temperature [*Broecker and Peng*, 1982; *Broecker et al.*, 1978; *Quay et al.*, 1983; *Wanninkhof et al.*, 1995; *Klein and Rhein*, 2004; *Rhein et al.*, 2010; *Steinfeldt et al.*, 2015; *Kadko and Johns*, 2011; *Haskell et al.*, 2015]. Recently, two tracers have shown promise in estimating upwelling rates over the mesoscale range. In one, observations of helium isotopic disequilibrium in surface mixed layers have been used to derive upwelling rates of ~1–2 m/d in the equatorial Atlantic [*Klein and Rhein*, 2004; *Rhein et al.*, 2010] and ~1–3 m/d in coastal upwelling regions off Peru and Mauritania [*Steinfeldt et al.*, 2015]. This method relies on accurate assessment of the gas exchange rate and vertical diffusivity at the base of the mixed layer. The other method, used in this work, utilizes observed dilution of ^{7}Be in the surface mixed layer, resulting from upwelling of ^{7}Be-deficient water from depth, to infer upwelling rates. The shape of the ^{7}Be profile is used to derive vertical diffusivities in the upper thermocline. Derivations of this approach have been described in detail elsewhere [*Kadko and Johns*, 2011; *Haskell et al.*, 2015], and results therein are comparable to those derived from the δ^{3}He method.

The model is shown schematically in Figure 4 where the upper ocean consists of a surface mixed layer with constant ^{7}Be concentration (C_o) and an underlying "tail" layer where the ^{7}Be concentration $C(z)$ decays to zero at some depth z_o. *Kadko and Johns* [2011] derived a simple case for w_H, which is the upwelling rate at the base of the mixed layer and is assumed to be constant to the depth where the ^{7}Be signal vanishes. If F is the atmospherically derived ^{7}Be surface flux into the mixed layer, λ is the ^{7}Be decay constant (0.013 day^{-1}), H is the mixed layer depth, and C_{inv} is the total water column ^{7}Be inventory, then

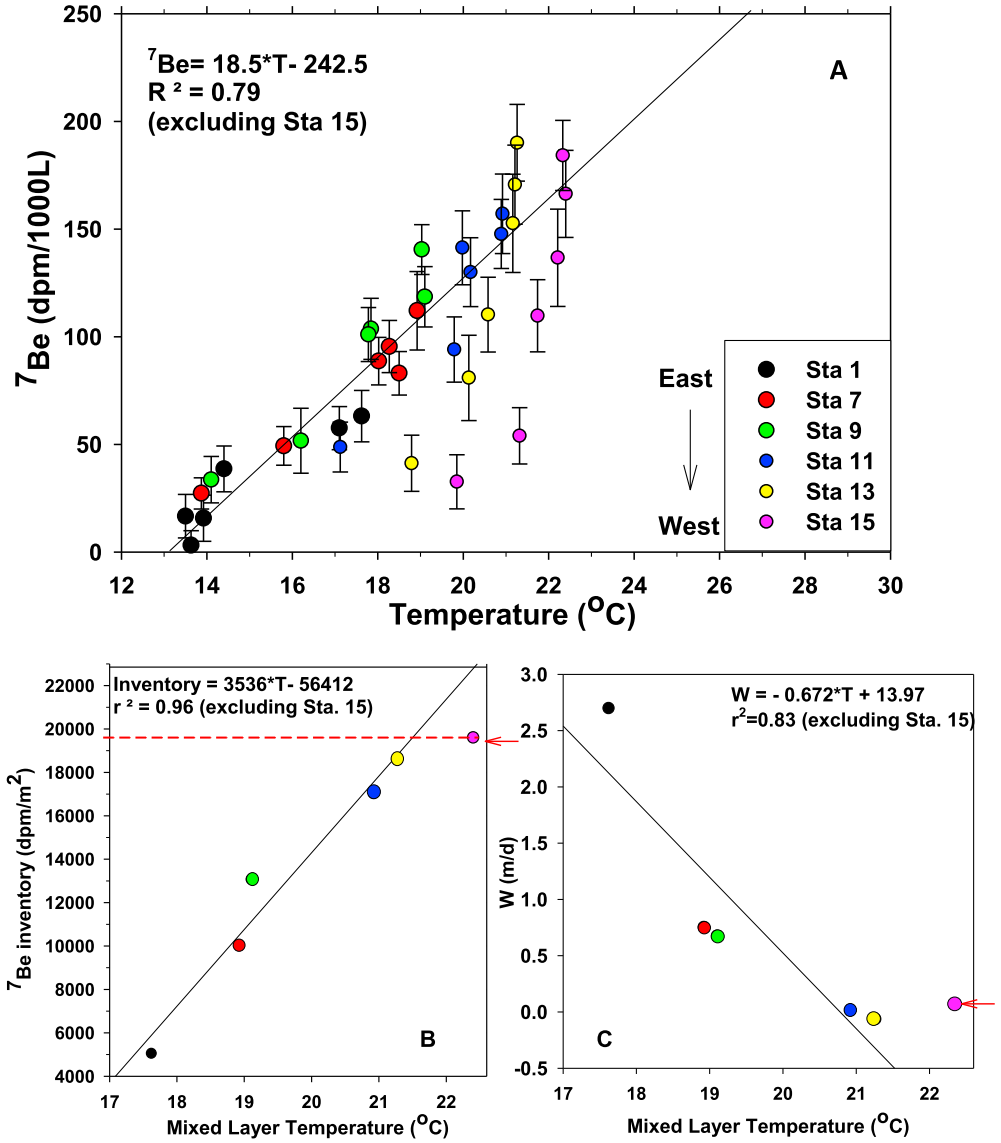

Figure 3. (a) ^{7}Be activities plotted against temperature from station profiles. (b) ^{7}Be inventories plotted against mixed layer temperature. The horizontal dashed line indicates the inventory from nonupwelling stations and represents the atmospheric ^{7}Be input. (c) Calculated upwelling rate (W) plotted against mixed layer temperature using equation (2) with $u = 0.1$ m/s. The red arrow indicates stations not affected by upwelling.

$$w_H = \frac{1}{C_o}(F - \lambda C_{\text{inv}}) \tag{1}$$

Note that when upwelling is negligible, $F = \lambda C_{\text{inv}}$, which represents a balance between the atmospheric input of ^{7}Be to the ocean and its radioactive decay inventory. Thus, the depth-integrated decay (inventory) of ^{7}Be at nearby, nonupwelling stations can be used to estimate the regional ^{7}Be flux (F) required for equation (1). The point is that the "deficit" of the ^{7}Be inventory of upwelling stations relative to nonupwelling stations can provide a measure of the upwelling rate. For this study, we use the ^{7}Be inventory of station 15 as representative of the atmospheric flux for the region of upwelling. Figure 3b shows that moving offshore, as temperature within the mixed layer increases, a "steady" inventory of ^{7}Be is approached for nonupwelling stations 13 and 15.

In earlier works [*Kadko and Johns*, 2011; *Haskell et al.*, 2015], horizontal advection of ^{7}Be into the mixed layer was ignored although it was suggested that in some cases errors in doing so could reach 30% [*Kadko and*

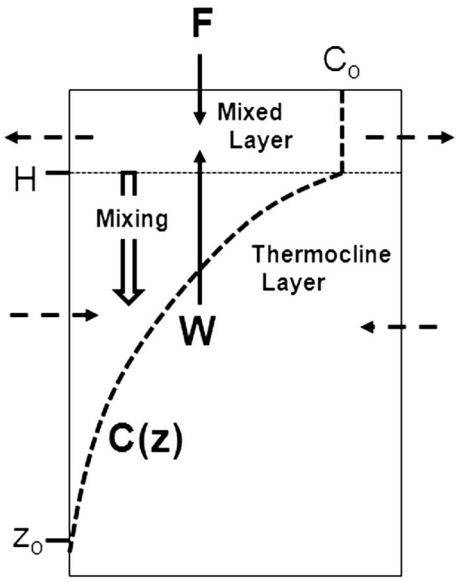

Figure 4. Conceptual model used in upwelling calculation [from *Kadko and Johns*, 2011]. $C_o = [^7Be]$ mixed layer concentration, $C_{zo} = [^7Be] = 0$ at depth Z_o, w = constant upwelling velocity through the upper thermocline (m/d), and H = depth of mixed layer (m). The dashed line is the ^7Be concentration profile (C_z) internal to the box comprising the mixed layer and the upper thermocline. The dashed arrows indicate relative divergence of horizontal flow in the mixed layer and the convergence in the thermocline.

Johns, 2011]. Here, given the relatively well-resolved horizontal station spacing, and some knowledge of horizontal velocity [u estimated as 0.1 m/s from *Huyer et al*., 1987; *Fiedler et al*., 1991; *Meinen et al*., 2001; *Lumpkin and Johnson*, 2013], equation (1) can be corrected for horizontal advection:

$$w_H = \frac{1}{C_o}\left(F - \lambda C_{\text{inv}} - H\bullet[u\delta C/\delta x]\right) \tag{2}$$

The effect of the westward flow is generally to bring low-^7Be water to offshore stations, leading equation (1) to overestimate w_H. The effect of eddies propagating westward at 0.03–0.06 m/s [*Chaigneau et al*., 2008] is not considered here. Table 2 summarizes this calculation and indicates that the advective term can be as high as 16% of the atmospheric flux for $u = 0.1$ m/s. The upwelling rate for the case of $u = 0.1$ m/s is plotted on the map of Figure 1 and against temperature in Figure 3c. The results here are comparable to those from approximately the same study area presented by *Steinfeldt et al*. [2015], using ^3He disequilibrium, and by *Haskell et al*. [2015] who applied ^7Be measurements to this model (but neglecting horizontal transport). Of note, the control or nonupwelling station inventory determined in the Haskell et al. work was within 20% of that determined from station 15 here.

Table 2. Upwelling Rates w_H Determined by Uniform Upwelling Model With Horizontal Advection[a]

	$u = 0$ m/s[b]		$u = 0.05$ m/s[b]		u = 0.1 m/s[b]		$u = 0.2$ m/s[b]	
Station	w_H	Horiz Flux[c]/F	w_H	Horiz Flux[c]/F	w_H	Horiz Flux[c]/F	w_H	Horiz Flux[c]/F
1	3.0	0	2.9	−0.04	2.7	−0.08	2.4	−0.15
7	1.1	0	0.93	−0.08	0.75	−0.16	0.39	−0.32
9	0.72	0	0.70	−0.01	0.68	−0.02	0.63	−0.04
11	0.22	0	0.12	−0.06	0.02	−0.125	−0.19	−0.25
13	0.07	0	0.0	−0.05	−0.06	−0.10	−0.20	−0.20
15	0	0	0.05	0.03	0.09	0.06	0.18	0.13

[a] w_H in m/d.
[b] Horizontal advection to the west.
[c] The ratio of horizontal advective flux to the atmospheric input flux.

Table 3. Upwelling Rates Determined by Depth-Dependent Upwelling Model With Horizontal Advection

		$u = 0.0$ m/s	$u = 0.05$ m/s	$u = 0.1$ m/s	$u = 0.2$ m/s
Station	Z_w (m)[a]	w_H[b]	w_H[b]	w_H[b]	w_H[b]
1	142	4.9	4.6	4.4	3.9
7	150	2.0	1.7	1.3	0.70
9	154	1.65	1.6	1.5	1.4
11	152	0.51	0.275	0.04	−0.43
13	153	0.135	0.01	−0.12	−0.37
15	173	0	0.08	0.15	0.30

[a]Depth where w is zero at 100 m below the base of the mixed layer.
[b]$w_H = w$ at the base of mixed layer.

The w_H estimate derived from equations (1) and (2) is a lower bound, as the actual w_H will be higher if the upwelling velocity is not constant but decreases with depth. This is more realistic, as it is expected that vertical velocity decreases over a finite vertical scale of the order 100 m below the mixed layer [e.g., *Huyer et al*., 1987; *Harrison*, 1996; *Kadko and Johns*, 2011] due to horizontal convergence within the thermocline. This needs to be considered when determining vertical transport of nutrients into the euphotic zone, particularly as the base of the euphotic zone is deeper than the base of the mixed layer for our stations [*Ohnemus et al*., 2016]. The simplest case is where w decreases linearly to zero over a depth scale Z_w below the mixed layer [e.g., *Quay et al*., 1983]. The formulation for ^{7}Be is described in *Kadko and Johns* [2011]:

$$w_H = (F - \lambda C_{\text{inv}}) / \left[C_o - \frac{1}{Z_w} \int_{z_o}^{H} C(z) dz \right] \tag{3a}$$

As was the case for constant w with depth, equation (3a) can be corrected for horizontal advection:

$$w_H = (F - \lambda C_{\text{inv}} - H \cdot [u \delta C / \delta x]) / \left[C_o - \frac{1}{Z_w} \int_{z_o}^{H} C(z) dz \right] \tag{3b}$$

These results are presented in Table 3.

There are several factors which contribute to the uncertainty of the upwelling calculations. For any of the model approaches, the ^{7}Be inventories (Table 1) contribute 4–9% uncertainty to the upwelling calculation. The ^{7}Be flux (F) term, which is based on the station chosen to represent the control inventory, presents further uncertainty. For example, the inventory of station 13 is approximately 6% less than that of station 15. If station 13, rather than station 15, is used as the control inventory, then the upwelling rate is reduced for all stations by 0.07–0.22 m/d using equation (2). The choice of the horizontal advection term (u) also contributes to the uncertainty. Again, considering equation (2), a difference of 0.05 m/s leads to a 0.1–0.2 m/d difference in upwelling velocity. Finally, the derived upwelling rates are somewhat model dependent. A comparison of Tables 2 and 3 indicates for example that w_H (upwelling at the base of the mixed layer) for the linearly decreasing w model can be twice as great as that of the constant w model. However, as discussed in the following section, the upwelling rate of the linearly decreasing w model at the depth chosen for the base of the euphotic zone is nearly identical to that of the constant w model. Thus, the model choice has minimal implication for nutrient flux and new production estimates.

3.2. Estimating Vertical Diffusion in the Upper Thermocline

The shape of the ^{7}Be profile beneath the mixed layer can be approximated by the one-dimensional vertical advection-diffusion equation with a radioactive decay term, where K_z is the vertical mixing coefficient [e.g., *Kadko and Johns*, 2011].

Table 4. Vertical Diffusion Coefficients (K_z)

		Constant w Model, $u = 0.1$ m/s		Linearly Decreasing w Model		
Station	α	K_z (10^{-4} m^2/s)	w_H	Z_c[a]	w[b]	K_z (10^{-4} m^2/s)
1	0.076	4.4	2.7	80	2.7	4.4
7	0.030	4.5	0.75	94	0.75	4.5
9	0.034	3.55	0.68	110	0.68	3.55
11	0.030	1.7	0.02	140	0.005	1.7
13	0.023	2.5	−0.06	147	−0.01	2.8
15	0.023	3.3	0.09	167	0.01	2.9

[a] Z_c is depth (PPZ) where the fluorescence trace first crosses the 10% level.
[b] Upwelling rate at Z_c.

$$\frac{\partial}{\partial z}\left(K_z \frac{\partial C}{\partial z}\right) - \lambda C - w\frac{\partial C}{\partial z} = 0 \tag{4}$$

For constant w (>0 for upwelling) and K_z over the ^{7}Be tail layer beneath the mixed layer, a simple exponential solution is derived:

$$C_{(z)} = C_o e^{\alpha(z-H)} \tag{5}$$

where the depth attenuation coefficient is

$$\alpha = \frac{w}{2k_z} + \frac{1}{2}\left\{\left(\frac{w}{k_z}\right)^2 + \frac{4\lambda}{Kz}\right\}^{\frac{1}{2}} \tag{6}$$

The assessment of the upwelling rate w does not require consideration of vertical mixing or the shape of the ^{7}Be profile because only the integrated inventory is considered. Independently of that calculation, the ^{7}Be profiles are fit to equation (5) to derive α. Using the fitted value of α and the value of w derived from the station inventory allows K_z to be derived from equation (6). For the constant upwelling model, the case where $u = 0.1$ m/s is used. For the linearly decreasing w model, the case of $u = 0.1$ m/s is also used and K_z is approximated using equation (6) with the value of w at the depth of the euphotic zone for the purpose of calculating the nitrate flux and new production (sections 3.3 and 3.4). Values of α and K_z are shown in Table 4. The results indicate that the upwelling rate for the constant w model is nearly identical to that of the linearly decreasing w model at the depth chosen for the base of the euphotic zone (discussed in section 3.3), as are the derived values of K_z. Plots of ^{7}Be modeled by equation (5) are shown in Figure 5. For the stations nearest the shore (1–11), the model cannot fit the entire profile from the base of the mixed layer to depth, as discontinuities in the accompanying temperature profiles suggest the system is not strictly one-dimensional nor adhering to constant w and K_z over the entire profile. For example, *Brink et al*. [1983] discuss poleward undercurrents observed on and near the shelf, which cannot be resolved with this data set. However, for the depths around the base of the euphotic zone relevant to evaluating nutrient fluxes and primary production, the model performs well. The ^{7}Be profiles are quite sensitive to the assumed K_z values and provide a fairly strong constraint on the magnitude of the local vertical mixing. Values of K_z derived here are comparable to those reported by *Haskell et al*. [2015], and both works indicate a generally increasing trend of this parameter from the south to the north. It must be noted that the depth of the euphotic zone (section 3.3) for station 13 is 24 m deeper than the deepest ^{7}Be sample and likely resides in a different water mass as suggested by a plot of temperature-salinity (not shown). Thus, the K_z derived from this tracer for station 13 should be used with caution.

For comparison, K_z can be derived from the temperature profiles using the approach of *Craig* [1969], where the temperature at some depth T_z between an upper boundary $z = m$ and a deep boundary $z = o$ is given by

$$T_z = (T_m - T_o)\frac{[\exp(z/z^*) - 1]}{[\exp(z_m/z^*) - 1]} + T_o \tag{7}$$

The value z^* is the one-dimensional mixing parameter K_z/w. With w derived from ^{7}Be, profiles of T are generated for chosen values of K_z. These results are presented in Figure 5. Again, single values of K/w cannot provide a fit for the entire temperature profile for nearshore stations but provide a reasonable fit for the depths around the base of the euphotic zone for stations where $w > 0$ and yield values of K_z comparable to those

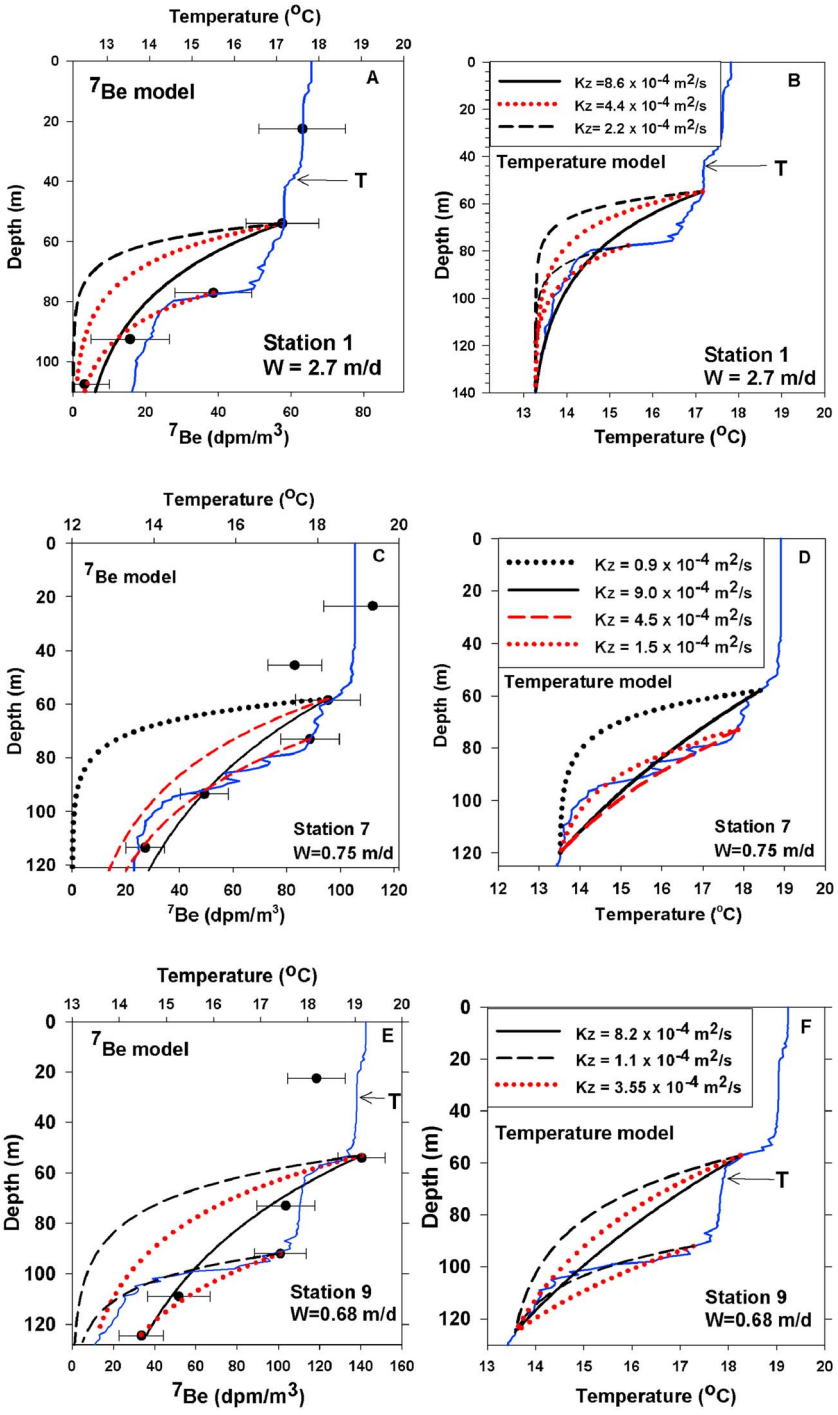

Figure 5. Plots of ^{7}Be modeled by equation (5): (a) station 1; (c) station 7; (e) station 9; (g) station 11; (i) station 13; (k) station 15. These are compared to the plots of temperature modeled by equation (7) and using w determined from the ^{7}Be method: (b) station 1; (d) station 7; (f) station 9; and (h) station 11. The station 11 result illustrates that as w approaches 0, the temperature profile becomes linear and K_z cannot be well resolved. For stations 1–11, ^{7}Be and temperature models are plotted for all depths beneath the mixed layer as well as for the best fit at depths near the euphotic zone. Temperature profiles generated by equation (7) using various values of K/w (see text): (j) station 13; (l) station 15.

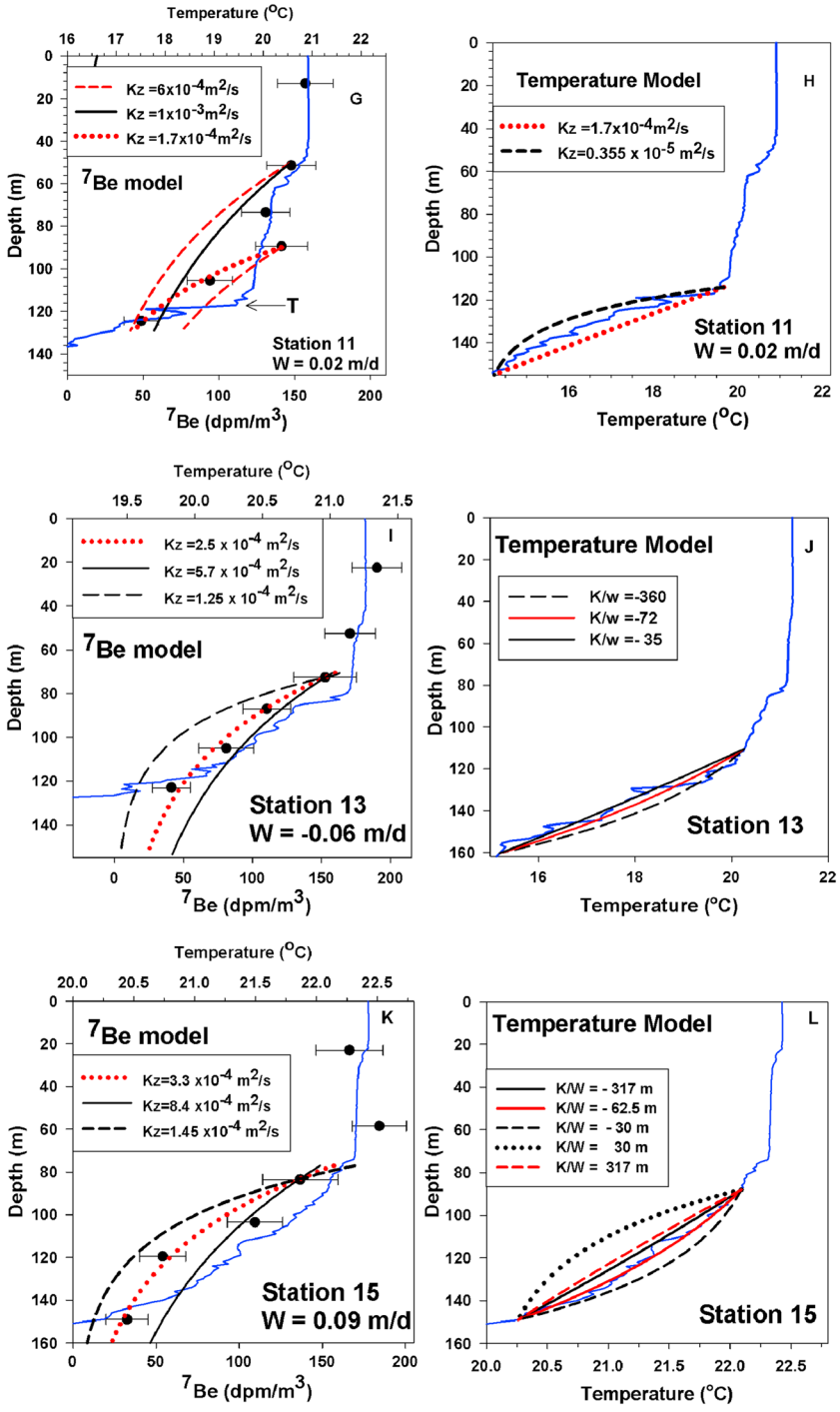

Figure 5. (continued)

derived from the ^{7}Be model (Figure 5, stations 1–9). Because temperature is a conservative tracer, as w approaches zero (i.e., diffusion only), the temperature profile becomes linear and K_z cannot be resolved [*Craig*, 1969]. This is illustrated in Figure 5h for station 11 where diffusion rates differing by a factor of 50 are not well resolved. For station 13 (Figures 5i and 5j), the temperature profile is linear between approximately 85 and 111 m depths. Apparent curvature below that interval results from intrusion of a different water mass as suggested by a plot of temperature-salinity mentioned above. Within the depth interval (111–160 m) encompassing the euphotic zone depth and deeper than the deepest ^{7}Be sample, temperature profiles generated by several values of K/w are plotted in Figure 5j. The line defined by $K/w = -360$ m represents the fit to the ^{7}Be

model (Figure 5i), where $w = -0.06$ m/d and $K_z = 2.5 \times 10^{-4}$ m^2/s. The line defined by $K/w = -72$ m yields $K_z = 0.5 \times 10^{-4}$ m^2/s. A factor of 5 difference of K_z is not well resolved by this method. For station 15, the temperature profile and profiles generated by several values of K/w are plotted in Figure 5l. The line defined by $K/w = 317$ m represents the fit to the ^{7}Be model (Figure 5k), where $w = 0.09$ m/d and $K_z = 3.3 \times 10^{-4}$ m^2/s. Values of K/w within the envelope defined by 317 m and -62.5 m are not readily distinguished from one another, but curvature of the temperature profile of station 15 corresponding to $K/w = -62.5$ may suggest downwelling. Based on the wind stress field, it has been estimated that downwelling at this site is ~ -0.1 to -0.2 m/d [*Risien and Chelton*, 2008]. Note that the difference between these values and the 0.09 m/d of the ^{7}Be model falls within the 0.1–0.2 m/d uncertainty of the ^{7}Be method discussed in section 3.1. If $K/w = -62.5$ m and $w = -0.2$ m/d, then $K_z = 1.45 \times 10^{-4}$ m^2/s, which is about half that determined by the ^{7}Be approach.

3.3. Nitrate Fluxes

Here the upwelling velocities (Table 3) and vertical eddy diffusivities (Table 4) derived in sections 3.1 and 3.2 are applied to nitrate profiles to estimate new production for the eastern section of the U.S. GEOTRACES East Pacific Zonal Transect (EPZT). The flux of nitrate at any depth z is given by

$$F_{NO3z} = w * [NO_3]_z + K_z*(\delta[NO_3]/\delta z)_z \quad (8)$$

The nitrate flux for each station is plotted as a function of depth in Figure 6. Depth variation in flux stems from the depth dependence of upwelling velocity, nitrate concentration, and gradient in nitrate concentration. Note that K_z is fixed at the value indicated in Table 4. While K_z may increase above the depth of the euphotic zone toward the base of the mixed layer [e.g., *Rhein et al*., 2010; *Kadko and Johns*, 2011], for these stations, the effect on the flux profile is small because the gradient in nitrate generally decreases as well.

The flux into the euphotic zone is

$$F_{NO3} = w * [NO_3]_c + K_z*(\delta[NO_3]/\delta z)_c \quad (9)$$

where $[NO_3]_c$ represents the nitrate concentration at the base of the euphotic zone. The euphotic zone is the depth range where daily gross primary production exceeds daily autotrophic respiration and thus net primary production exceeds zero and has been traditionally assumed to be the depth to which 1% of surface photosynthetically active radiation (PAR) remains. However, using ^{14}C estimation of net primary productivity, *Marra et al*. [2014] show that the compensation depth (Z_c) can be tens of meters deeper than the traditional 1% PAR definition. They suggest that Z_c will be more closely related to the depth that encompasses autotrophic biomass, indicated by in vivo fluorescence measurements, than the depth horizon of 1% of surface PAR. Similarly, *Chavez and Barber* [1987] suggested that in the eastern tropical Pacific primary production could be well estimated from accurate determinations of the depth distribution of chlorophyll. The data of *Marra et al*. [2014] suggest Z_c can occur from the base of the fluorescence maximum to where the fluorescence approaches the level of noise. More recently, the level where the fluorescence signal approaches 10% of the fluorescence maximum has been adopted as defining the euphotic zone, or the particle production zone (PPZ) [*Owens et al*., 2015; *Ohnemus et al*., 2016]. This definition is used here for the purpose of calculating the nitrate fluxes into the euphotic zone, which are presented in Table 5, but the reader can choose any depth of the flux profiles (and the corresponding flux) in Figure 6.

The net flux in Table 5 is calculated as the difference between the summed vertical transport terms and the horizontal export at the surface:

$$\text{Net } F_{NO3} = F_{NO3} - w_H[NO_3]_o \quad (10)$$

where $[NO_3]_o$ is the mixed layer nitrate concentration. A positive net F_{NO3} is determined for all stations at the PPZ except for station 7. At station 7, the horizontal export term exceeds the nitrate flux calculated at the PPZ (94 m, Tables 4 and 5). With the parameters chosen here, a positive net F_{NO3} is reached higher in the water column, at 70 m depth. For the offshore stations (11, 13, and 15), vertical advection is negligible such that vertical transport is dominated by turbulent diffusion. In this case, the nitrate flux is quite sensitive to the choice of K_z. For example, for station 13, while there is overlap of K_z values derived from the ^{7}Be and temperature models, the temperature model (equation (7)) suggests K_z could be a factor of 5 less than that derived from ^{7}Be; however, the resolution for the temperature model is poor for diffusive systems. For station 15, the temperature model suggests that K_z could be half that indicated by the ^{7}Be model; this would lower the estimate of new production discussed below.

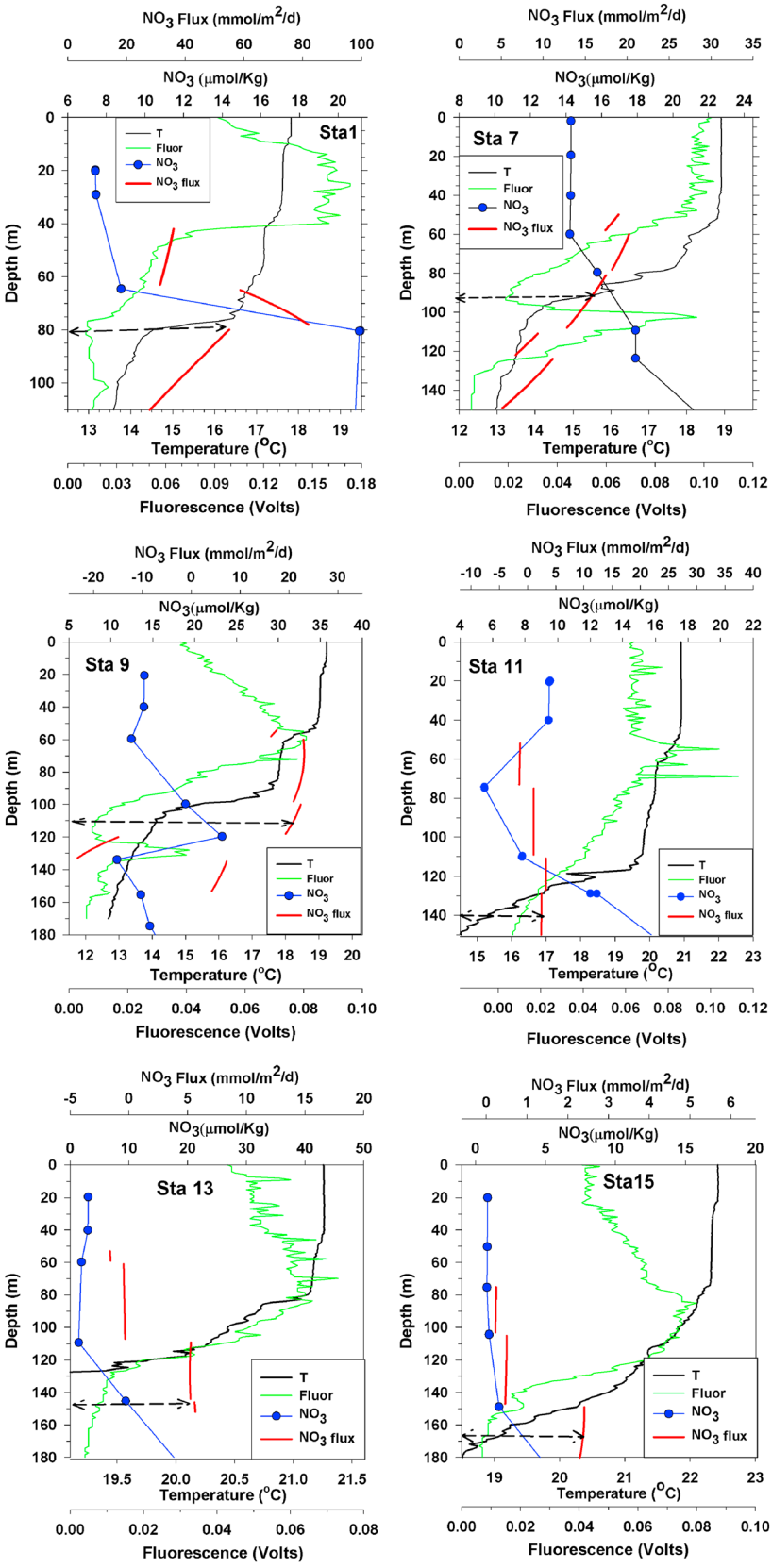

Figure 6. Temperature, fluorescence, NO_3, and NO_3 flux plotted again depth for the stations in this study. The horizontal dashed black arrow indicates the depth of the euphotic zone (see text).

Table 5. NO_3 Fluxes and NCP (mmol/m^2/d) at Z_c

	NO_3				
Station	Advected	Diffusive	Sum	Net[a]	NCP[b]
1	55.2	−0.30	54.9	20.3	134 (1.6)
7	12.6	2.8	15.4	<0[c]	-
9	14.3	6.7	21.0	1.1	7.3 (0.09)
11	0.07	2.38	2.45	2.1	14.1 (0.17)
13	−0.07	5.7	5.6	5.9	38.9 (0.47)[d]
15	0.03	2.35	2.4	2.25	14.9 (0.18)[d]

[a]Net nitrate flux into the euphotic zone, defined as the PPZ (see text).
[b]Net community production (mmol C/m^2/d) based on the net nitrate flux × 6.6. Numbers in parenthesis are in g C/m^2/d.
[c]With the parameters chosen here, a positive net nitrate flux at station 7 occurs higher in the water column (70 m) than the PPZ (94 m) and equals 0.1 mmol/m^2/d (see text).
[d]Analysis of the temperature model suggests these values are an upper limit (see text).

3.4. New Production

New production is estimated by multiplying the net nitrate flux by a C:N ratio of 6.6. The results are shown in Table 5. While there is no consensus on the best way to estimate new/export production [*Laws et al*., 2000], it is still instructive to compare the estimates here to literature values. Station 1, the furthest inshore station and that displaying the coldest SST, had by far the highest derived new production of 134 mmol C/m^2/d. This value is comparable to the 160 mmol C/m^2/d for the PCU based on estimated nitrate uptake using ^{15}N tracer [*Wilkerson et al*., 1987]. *Chavez and Barber* [1987] derived 95 mmol C/m^2/d for the Peru coast from ^{14}C uptake and an assigned *f* value (the ratio of new production to total production) of 0.5 based on *Eppley and Peterson* [1979] for high-productivity regions. *Laws et al*. [2000] present a value of *f* for Peru of 0.42 that would lower the Chavez and Barber estimate to 80 mmol C/m^2/d. *Pennington et al*. [2006] present a value of 298 mmol C/m^2/d for production in the PCU, which combined with the 134 mmol/m^2/d value of new production for station 1 derived here yields a value for *f* of 0.45.

The average new production determined by the ^{7}Be method for all stations west of station 1 is 15 mmol C/m^2/d. For stations where vertical transport is dominated by turbulent diffusion (particularly 13 and 15), analysis of temperature profiles suggests that this average represents an upper limit, although in such cases the resolution of the temperature model is poor. *Chavez and Barber* [1987] report a value of primary production for a zone west of 92°W between 3°N and 17°S of 42 mmol C/m^2/d and for a zone west of 85°W between 4°N and 10°S of 64 mmol C/m^2/d. Recognizing the problem of comparing measurements separated by time and different spatial extent, the implied range of *f* from the primary production measurements of Chavez and Barber and the ^{7}Be-derived new production estimates here is 0.23–0.36. *Fiedler et al*. [1991], using upwelling velocities estimated from divergence of horizontal transport, derived new production along 10°S, west of 81°W, of ~17 mmol C/m^2/d, comparable to that presented here. They also present a regional value for *f* of 0.29 ± 0.11. *Pennington et al*. [2006] present a value for primary production of 31.3 mmol/m^2/d for the eastern boundary current west of the PCU, which considered with the average new production west of station 1 here yields *f* = 0.48. For the equatorial Pacific between 170°W and 95°W, *Emerson* [2014] reports an average new production of 9 mmol C/m^2/d, which is derived from a compilation of various methods. Finally, *Haskell et al*. [2015], using an approach similar to that of this paper, derived new production of 19 mmol C/m^2/d for a station at 10°S, 100°W; the calculated new production for the nearest location to that site in this paper (station 13, 14°S, 99°W) is 38.9 mmol C/m^2/d.

Knapp et al. [2016] considered N_2 fixation as a factor in export production and showed that it is a minor source of new nitrogen to surface waters in this region, suggesting that the NO_3 flux should be representative of C export. It is therefore interesting to compare the calculated new production to the carbon export flux. *Black et al*. [submitted] derived POC fluxes, based on the ^{234}Th deficit method [e.g., *Buesseler et al*., 2006], for the EPZT stations. For both the nearshore and offshore regions, the POC flux is less than the new production calculated here. This is not unexpected, but the difference between the new production calculated here for nearshore station 1 (134 mmol C/m^2/d) is ~100 mmol C/m^2/d greater than the POC flux determined by Black et al. for station 1 as well as stations further inshore not discussed here. Earlier estimates of POC fluxes

from this region, also determined by the ^{234}Th deficit method, were similarly found to be quite low compared to estimates of primary production [*Haskell et al*., 2013]. *Plattner et al*. [2005] describe how export production can become spatially decoupled from new production because a fraction of the newly produced organic material can be transported laterally before leaving the euphotic zone, a process known to be particularly important in dynamic coastal upwelling systems. A rough calculation suggests that this could be the case here. For the nearshore stations of this study, the difference between mixed layer and deep DOC ~ 20 μM (C. Carlson, pers. comm.) and the difference between mixed layer and deep suspended total POC is ~10 μM (P. Lam, pers. comm.). Multiplying the sum of these terms by the upwelling rate (~4 m/d, which represents the divergence of horizontal flow in the mixed layer as shown in Figure 4) yields a potential lateral flux of 120 mmol/m^2/d, suggesting the importance of decoupling in this region.

4. Conclusions

Rates of upwelling and vertical diffusion within the upper thermocline were derived for stations between 79°W and 104°W along the U.S. GEOTRACES EPZT utilizing a previously developed method based on water column measurements of ^{7}Be. These transport terms were applied to nitrate profiles to estimate net community production within the zone of active upwelling to the edge of the oligotrophic gyre. The derived upwelling rates are somewhat model dependent. The constant *w*, one 1-dimensional model yielded calculated upwelling rates that were inversely related to mixed layer temperature and ranged from 0 to 3.0 m/d. Results using a depth-dependent upwelling rate with a component of horizontal advection were also developed, which led to higher upwelling rates at the base of the mixed layer. The upwelling rates derived from the constant *w* model were however nearly identical to the *w* of the depth-dependent model at the base of the euphotic zone, as were vertical diffusivities. Vertical diffusivities based on ^{7}Be profiles near the base of the euphotic zone were in the range 1.7–4.5 × 10^{-4} m^2/s. For nearshore stations, these values were comparable to those generated by analysis of temperature profiles. For offshore stations, analysis of temperature profiles suggests the ^{7}Be-derived values represent an upper limit, although for diffusion-dominated stations, the resolution of the temperature model is poor. Net community production derived here averages 15 mmol C/m^2/d for stations between 84°W and 104°W and is 134 mmol C/m^2/d for the furthest inshore station at 79°W which displayed the lowest SST and greatest rate of upwelling. These rates are comparable to those found in the literature based on other methods. For the nearshore stations export production can become spatially decoupled from new production because a fraction of the newly produced organic material can be transported laterally before leaving the euphotic zone. The tracer technique used here provides insight into the underlying physical transport which ultimately drives the new production. Higher-resolution sampling both offshore and along shore, in tandem with other tracers (such as ^{3}He), might better resolve the depth dependence of upwelling and source waters.

Acknowledgments

The author wishes to thank the captain and crew of R/V *Thomas G. Thompson* for their able field support. Mark Stephens provided important at-sea and laboratory technical assistance. Discussions with William Johns, William Jenkins, and Paul Quay were greatly appreciated. Comments by Douglas Hammond and an anonymous reviewer were very helpful. Data have been submitted to The Biological and Chemical Oceanography Data Management Office (BCO-DMO) and is accessible at http://www.bco-dmo.org/dataset/665158. This work was supported by the Chemical Oceanography Program of the NSF, grant OCE-1232794.

References

Aaboe, E., E. P. Dion, and K. K. Turekian (1981), ^{7}Be in Sargasso Sea and Long Island Sound waters, *J. Geophys. Res.*, *86*, 3255–3257, doi:10.1029/JC086iC04p03255.

Black, E. E., K. O. Buesseler, S. M. Pike, and P. J. Lam (submitted), ^{234}Th as a tracer of particulate export and remineralization in the Southeastern Tropical Pacific, *Mar. Chem.*

Brink, K. H., D. Halpern, A. Huyer, and R. L. Smith (1983), The physical environment of the Peruvian upwelling system, *Progr. Oceanogr.*, *12*, 285–305.

Broecker, W. S., and T.-H. Peng (1982), *Tracers in the Sea*, 690 pp., Eldigio Press, Palisades, New York.

Broecker, W. S., T. H. Peng, and M. Stuiver (1978), An estimate of the upwelling rate in the equatorial Atlantic based on the distribution of bomb radiocarbon, *J. Geophys. Res.*, *83*, 6179–6186, doi:10.1029/JC083iC12p06179.

Buesseler, K. O., et al. (2006), An assessment of particulate organic carbon to thorium-234 ratios in the ocean and their impact on the application of ^{234}Th as a POC flux proxy, *Mar. Chem.*, *100*, 213–233, doi:10.1016/j.marchem.2005.10.013.

Chaigneau, A., A. Gizolme, and C. Grados (2008), Mesoscale eddies off Peru in altimeter records: Identification algorithms and eddy spatio-temporal patterns, *Progr. Oceanogr.*, *79*, 106–119.

Chavez, F. P., and R. T. Barber (1987), An estimate of new production in the equatorial Pacific, *Deep Sea Res.*, *34*, 1229–1243.

Craig, H. (1969), Abyssal carbon and radiocarbon in the Pacific, *J. Geophys. Res.*, *74*, 5491–5506, doi:10.1029/JC074i023p05491.

Emerson, S. (2014), Annual net community production and the biological carbon flux in the ocean, *Global Biogeochem. Cycles*, *28*, 14–28, doi:10.1002/2013GB004680.

Eppley, R. W., and B. J. Peterson (1979), Particulate organic matter flux and planktonic new production m the deep ocean, *Nature*, *282*, 677–680.

Fiedler, P. C., and L. D. Talley (2006), Hydrography of the eastern tropical Pacific: A review, *Progr. Oceanogr.*, *69*, 143–180.

Fiedler, P. C., V. Philbrick, and F. P. Chavez (1991), Oceanic upwelling and productivity in the Eastern Tropical Pacific, *Limnol. Oceanogr.*, *36*, 1834–1850.

Fuenzalida, R., W. Schneider, J. Garcés-Vargas, L. Bravo, and C. Lange (2009), Vertical and horizontal extension of the oxygen minimum zone in the eastern South Pacific Ocean, *Deep Sea Res., Part II*, *56*, 992–1003.
Harrison, D. E. (1996), Vertical velocity in the central tropical Pacific: A circulation model perspective for JGOFS, *Deep Sea Res., Part II*, *43*, 687–705.
Haskell, W. Z., W. Berelson, D. E. Hammond, and D. G. Capone (2013), Particle sinking dynamics and POC fluxes in the Eastern Tropical South Pacific based on ^{234}Th budgets and sediment trap deployments, *Deep Sea Res., Part I*, *81*, 1–13.
Haskell, W. Z., D. Kadko, D. E. Hammond, A. N. Knapp, M. G. Prokopenko, W. M. Berelson, and D. G. Capone (2015), Upwelling velocity and eddy diffusivity from ^{7}Be measurements used to compare vertical nutrient flux to export POC flux in the Eastern Tropical South Pacific, *Mar. Chem.*, doi:10.1016/j.marchem.2014.10.004.
Huyer, A., R. L. Smith, and T. Paluszkiewicz (1987), Coastal upwelling off Peru during normal and El Niño times. 1981–1984, *J. Geophys. Res.*, *92*, 14,297–14,301, doi:10.1029/JC092iC13p14297.
Kadko, D. (2000), Modeling the evolution of the arctic mixed layer during the Fall 1997 SHEBA project using measurements of ^{7}Be, *J. Geophys. Res.*, *105*, 3369–3378, doi:10.1029/1999JC900311.
Kadko, D. (2009), Rapid oxygen utilization in the ocean twilight zone assessed with the cosmogenic isotope ^{7}Be, *Global Biogeochem. Cycles*, *23*, GB4010, doi:10.1029/2009GB003510.
Kadko, D., and D. Olson (1996), Be-7 as a tracer of surface water subduction and mixed layer history, *Deep Sea Res.*, *43*, 89–116.
Kadko, D., and J. Prospero (2011), Deposition of ^{7}Be to Bermuda and the regional ocean: Environmental factors affecting estimates of atmospheric flux to the ocean, *J. Geophys. Res.*, *116*, C02013, doi:10.1029/2010JC006629.
Kadko, D., and W. Johns (2011), Inferring upwelling rates in the equatorial Atlantic using ^{7}Be measurements in the upper ocean, *Deep Sea Res., Part I*, *58*, 247–257, doi:10.1016/j.dsr.2011.03.004.
Kadko, D., W. M. Landing, and R. U. Shelley (2015), A novel tracer technique to quantify the atmospheric flux of trace elements to remote ocean regions, *J. Geophys. Res. Oceans*, *119*, 848–858, doi:10.1002/2014JC010314.
Karstensen, J., L. Stramma, and M. Visbeck (2008), Oxygen minimum zones in the eastern tropical Atlantic and Pacific oceans, *Prog. Oceanogr.*, *77*, 331–350.
Klein, B., and M. Rhein (2004), Equatorial upwelling rates inferred from helium isotope data: A novel approach, *Geophys. Res. Lett.*, *31*, L23308, doi:10.1029/2004GL021262.
Knapp, A. N., K. L. Casciotti, W. M. Berelson, M. G. Prokopenko, and D. G. Capone (2016), Low rates of nitrogen fixation in eastern tropical South Pacific surface waters, *Proc. Natl. Acad. Sci. U.S.A.*, *113*(16), 4398–4403.
Krishnaswami, S., D. Lal, B. L. K. Somayajulu, F. S. Dixon, S. A. Stonecipher, and H. Craig (1972), Silicon, radium, thorium and lead in seawater: In-situ extraction by synthetic fibre, *Earth Planet. Sci. Lett.*, *16*, 84–90.
Lal, D., Y. Chung, T. Platt, and T. Lee (1988), Twin cosmogenic radiotracer studies of phosphorus recycling and chemical fluxes in the upper ocean, *Limnol. Oceanogr.*, *336*, 1559–1567.
Laws, E. A., P. G. Falkowski, W. O. Smith, H. Ducklow, and J. J. McCarthy (2000), Temperature effects on export production in the open ocean, *Global Biogeochem. Cycles*, *14*, 1231–1246, doi:10.1029/1999GB001229.
Lee, T., E. Barg, and D. Lal (1991), Studies of vertical mixing in the Southern California Bight with cosmogenic radionuclides ^{32}P and ^{7}Be, *Limnol. Oceanogr.*, *365*, 1044–1053.
Lumpkin, R., and G. C. Johnson (2013), Global ocean surface velocities from drifters: Mean, variance, El Nino-Southern Oscillation response, and seasonal cycle, *J. Geophys. Res. Oceans*, *118*, 2992–3006, doi:10.1002/jgrc.20210.
Marra, J. F., V. P. Lance, R. D. Vaillancourt, and B. R. Hargreaves (2014), Resolving the ocean's euphotic zone, *Deep Sea Res., Part I*, *83*, 45–50, doi:10.1016/j.dsr.2013.09.005.
Meinen, C. S., M. J. McFaden, and G. C. Johnson (2001), Vertical velocities and transports in the equatorial Pacific during 1993–99, *J. Phy. Ocean.*, *31*, 3230–3248.
Montecino, V., and C. B. Lange (2009), The humboldt current system: Ecosystem components and processes, fisheries, and sediment studies, *Prog. Oceanogr.*, *83*, 65–79.
Ohnemus, D. C., Rauschenberg, S., Cutter, G. A., Fitzsimmons, J. N., Sherrell, R. M., and Twining, B. S. (2016), Elevated trace metal content of prokaryotic communities associated with marine oxygen deficient zones, *Limnol. Oceanogr.*, doi:10.1002/lno.10363. (in press)
Owens, S. A., S. Pike, and K. O. Buesseler (2015), Thorium-234 as a tracer of particle dynamics and upper ocean export in the Atlantic Ocean, *Deep Sea Res., Part II*, *116*, 42–59, doi:10.1016/j.dsr2.2014.11.010.
Pennington, J. T., K. L. Mahoney, K. S. Kuwahara, D. D. Kolber, R. Calienes, and F. P. Chavez (2006), Primary production in the eastern tropical Pacific: A review, *Progr. Oceangr.*, *69*, 285–317.
Plattner, G.-K., N. Gruber, H. Frenzel, and J. C. McWilliams (2005), Decoupling marine export production from new production, *Geophys. Res. Lett.*, *32*, L11612, doi:10.1029/2005GL022660.
Quay, P. D., M. Stuiver, and W. S. Broecker (1983), Upwelling rates for the equatorial Pacific Ocean derived from the bomb ^{14}C distribution, *J. Mar. Res.*, *41*, 769–792.
Rhein, M., M. Dengler, J. Sültenfuß, R. Hummels, S. Hüttl-Kabus, and B. Bourles (2010), Upwelling and associated heat flux in the equatorial Atlantic inferred from helium isotope disequilibrium, *J. Geophys. Res.*, *115*, C08021, doi:10.1029/2009C005772.
Risien, C. M., and D. B. Chelton (2008), A global climatology of surface wind and wind stress fields from eight years of QuikSCAT scatterometer data, *J. Phys. Ocean.*, *38*, 2379–2413.
Silker, W. B. (1972), Beryllium-7 and fission products in the GEOSECS II water column and applications of their oceanic distributions, *Earth Planet. Sci. Lett.*, *16*, 131–137.
Steinfeldt, R., J. Sültenfuß, M. Dengler, T. Fischer, and M. Rhein (2015), Coastal upwelling off Peru and Mauritania inferred from helium isotope disequilibrium, *Biogeosciences*, *12*, 7519–7533.
Wanninkhof, R., R. A. Feely, D. K. Atwood, G. Berberian, D. Wilson, P. P. Murphy, and M. F. Lamb (1995), Seasonal and lateral variations in carbon chemistry of surface water in the eastern equatorial Pacific during 1992, *Deep Sea Res., Part II*, *42*, 387–409.
Wilkerson, F. P., R. C. Dugdale, and R. T. Barber (1987), Effects of El Niño on new, regenerated and total production in eastern boundary upwelling systems, *J. Geophys. Res.*, *14*, 14,347–14,353, doi:10.1029/JC092iC13p14347.
Young, J. A., and W. B. Silker (1980), Aerosol deposition velocities on the Pacific and Atlantic Oceans calculated from ^{7}Be measurements, *Earth Planet. Sci. Lett.*, *50*, 92–104.